

Article

Multi-Disturbance Observers-Based Nonlinear Control Scheme for Wire Rope Tension Control of Hoisting Systems with Backstepping

Wanshun Zang ¹ , Xiao Chen ² and Jun Zhao ^{1,*}

¹ College of Mechanical and Electronic Engineering, Shandong University of Science and Technology, Qingdao 266590, China

² School of Mining Engineering, Anhui University of Science and Technology, Huainan 232000, China

* Correspondence: skdzhaojun@sdust.edu.cn

Abstract: The objective of this paper is to pursue a wire rope control methodology for reducing the tension difference between two wire ropes of a hoisting system. As we know, complicated disturbances exist in the complex electro-hydraulic hoisting system, notably, some of these disturbances are coupled, such as high-speed airflow disturbances, structure vibrations and vibrations in flexible wire ropes. Furthermore, there are model errors in force modeling due to the Coulomb friction between two wire ropes and two moveable head sheaves in the real physical hoisting systems. To eliminate disturbances, two types of disturbance observers (DOs) are employed: a traditional disturbance observer (TDO) and a coupled disturbance observer (CDO), both of which are utilized to estimate and compensate for the Coulomb friction and coupled disturbances online. As a result, a nonlinear backstepping control scheme is presented with estimation values from the TDO and the CDO. The experiment's results demonstrate the effectiveness of the proposed control methodology.



Citation: Zang, W.; Chen, X.; Zhao, J. Multi-Disturbance Observers-Based Nonlinear Control Scheme for Wire Rope Tension Control of Hoisting Systems with Backstepping. *Actuators* **2022**, *11*, 321. <https://doi.org/10.3390/act11110321>

Academic Editor: Tatiana Minav

Received: 9 October 2022

Accepted: 4 November 2022

Published: 6 November 2022

Publisher's Note: MDPI stays neutral with regard to jurisdictional claims in published maps and institutional affiliations.



Copyright: © 2022 by the authors. Licensee MDPI, Basel, Switzerland. This article is an open access article distributed under the terms and conditions of the Creative Commons Attribution (CC BY) license (<https://creativecommons.org/licenses/by/4.0/>).

Keywords: wire rope tension control; disturbance observer; backstepping

1. Introduction

Hoisting systems are common wire rope transmission systems that have been widely used in a variety of applications, such as high-speed elevators [1], mine hoisting [2,3], large-scale offshore platforms [4], crawler cranes [5] and so on. Wire ropes are the unique transmission carrier in hoisting systems. It is critical to understand how to guarantee load mass balance in order to reduce the wear and tear of wire ropes, which will prolong the service life of the wire ropes. Both passive and active coordination systems (ACSs) can balance the load mass [2] in wire ropes. To coordinate the wire ropes' tension, most hoisting systems employ passive devices such as a dancer arm, a hysteresis brake, or two suspended hydraulic cylinders with a communication vessel [2,6]. However, as the hoisting velocity increases, these passive devices are no longer adequate for quick response to multi-wire ropes' tensions [6,7]. The ACS, on the other hand, is faster and more efficient than passive coordination systems [3]. Additionally, the ACS, combining some active control methodologies, can ensure load balance among multi-wire ropes [8], thereby extending the service life of wire ropes and reducing wire rope vibrations [9].

Without the ACS model, a proportional-integral (PI) controller can coordinate wire rope tensions [10]. However, the PI controller's performance is never satisfactory. For instance, in Refs. [2,8], PI controllers are conducted on electro-hydraulic servo systems to actively coordinate two wire rope tensions. However, tension differences between two wire ropes are bigger than the model-based control schemes. Therefore, many model-based controllers are meant to produce higher performance by developing the ACS model. Adaptive controllers [11–13], robust controllers [14–16], and sliding mode controllers [17–20] are among the approaches developed. Adaptive controllers employ online parameter update

approaches or neural network-based adaptive techniques to derive the projection mapping between the adaptive law and some state variables. Robust controllers are designed using MATLAB or other comparable software with linear matrix inequality tools to make them robust to lumped system uncertainties, including disturbances and parameter uncertainties. Sliding mode controllers can be created by employing different sliding mode surfaces to achieve various control goals. All of these controllers are capable of coordinating wire rope tensions. Backstepping controllers (BCs) can be developed by dividing a system state space model into several subsystems, enabling virtual control laws and the real control law to be derived if proper Lyapunov functions are defined according to control goals [21–24]. Since backstepping techniques deeply analyze the system model, controllers based on backstepping techniques exhibit better performance than the controllers mentioned previously.

However, hoisting systems are mostly employed in challenging environments, many of which will provide complicated disturbances such as high-speed airflow disturbances, structural vibrations, and vibrations in flexible wire ropes, all of which result in difficulties for control performance. Disturbance observers (DOs) are effective tools for dealing with disturbances [25,26], as evidenced by types of DOs such as extended DOs [27], high-gain DOs [21], sliding mode DOs [28,29] and traditional disturbance observers (TDOs) [30–32]. What's more, estimation values from these DOs can be employed in controllers including sliding mode controllers [33–35] and backstepping controllers [24,36] to achieve better performance. However, if a system in severe environments has n actuators ($n \geq 2$), coupled disturbances will be broadcast throughout a mechanical network of n actuators, which will amplify the effect of coupled disturbances. DOs mentioned above are unsatisfactory to cope with coupled disturbances. As a result, Guo [37] addressed the CDO for multi-electro-hydraulic actuator systems and provided an excellent solution for coupled disturbance suppression. Combining the estimation value of the CDO, backstepping controllers can be derived.

Inspired by the above research, a new model and control approach is proposed for tension coordination of the ACS to achieve noncoupled and coupled disturbances suppression. The main contributions of the paper can be summarized as:

- (1) A differentiable tension model suited for nonlinear control is developed by taking the force model errors into account. By considering coupled disturbances in two hydraulic actuators, a differentiable speed model representing the transmission properties of coupled disturbances is established. Finally, a novel model for the ACS is derived by considering the noncoupled and coupled disturbances.
- (2) To mitigate the detrimental impact of noncoupled and coupled disturbances, a TDO and a CDO are proposed to estimate the nonlinear mapping element of the model and compensate for nonlinear uncertainty, resulting in a smaller tension difference.
- (3) To combine the TDO and the CDO with the backstepping controller, the tension derivative is chosen as the ACS's state variable to release the displacement term. To demonstrate the stability of the proposed control method, proper Lyapunov functions are developed.
- (4) To verify the proposed control methodology, a series of experimental studies are conducted on the experimental test rig. Comparative experimental results show that the proposed controller exhibits a better performance than a CDO based BC, a TDO based BC, a BC, or a conventional PI controller.

The remainder of the paper is structured as follows. Problem formulation and preliminaries are addressed in Section 2. The MDOBC is presented in Section 3. Section 4 compares some experimental results. Section 5 summarizes the primary conclusion.

2. Problem Formulation and Preliminaries

As shown in Figure 1, 1 and 2 denote the corresponding active coordination mechanism including the No. 1 hydraulic cylinder (N1HC), the No. 2 hydraulic cylinder (N2HC), and

the No. i moveable head sheave, and the No. i wire rope. The force F_{xi} is the resultant force of the tension from the vertical side (F_{zi}) and the tension from the catenary side ($F_{fi} + F_{zi}$).

$$F_{xi} = F_{zi} + (F_{zi} + F_{fi}) \sin \gamma_i, \quad i = 1, 2. \tag{1}$$

where, γ_i is the angle between the catenary wire rope and the upper plane and $\gamma_i \in [0, \pi/2]$ and F_{xi} is the force of the No. i hydraulic cylinder. F_{zi} is the No. i wire rope tension. According to Hooke’s law [38],

$$F_{xi} = k_f x_{pi} - k_f x_{pfi} \tag{2}$$

where, k_f is the stiffness, x_{pi} is the displacement of the No. i hydraulic cylinder, x_{pfi} is the displacement of the No. i movable head sheave. The time derivative of Equation (1) yields

$$\dot{F}_{zi} = k_f (\dot{x}_{pi} - \dot{x}_{pfi}) / (1 + \sin \gamma_i) + \Delta_i \tag{3}$$

where, $\Delta_i = -\dot{F}_{fi} \sin \gamma_i / (1 + \sin \gamma_i)$. If one considers the force balance in two hydraulic cylinders, one can derive the following equation.

$$A_p P_{Li} - F_{zi}(1 + \sin \gamma_i) = m_i \ddot{x}_{pi} + B_{pi} \dot{x}_{pi} + m_i d_{hi} \tag{4}$$

where, A_p is the effective area, $P_{Li} = p_{i1} - p_{i2}$ is the load pressure, m_i is the load mass, B_{pi} is the damping coefficient, $d_{h1} = (F_{f1} \sin \gamma_1 + F_{g1}) / m_1 + d_{12}$, $d_{h2} = (F_{f2} \sin \gamma_2 + F_{g2}) / m_2 + d_{21}$, d_{hi} is the total disturbance and d_{12} and d_{21} are the coupled disturbances. The load flow Q_{Li} yields

$$Q_{Li} = A_p \dot{x}_{pi} + V_{ti} \dot{P}_{Li} / 4\beta_e + C_{tli} P_{Li} \tag{5}$$

where, C_{tli} is the total leakage coefficient and V_{ti} is the total volume. Generally, the load flow $Q_{Li} = (Q_{1i} + Q_{2i}) / 2$ is controlled by the spool displacement x_{vi} of the corresponding servo valve; therefore,

$$Q_{Li} = C_d w x_{vi} \sqrt{(p_s - \text{sign}(x_{vi}) P_{Li}) / \rho_o} \tag{6}$$

where, C_d is the discharge coefficient, w is the throttle area gradient, ρ_o is the density of the supply oil and p_s is the supply pressure. According to Ref. [24], the control voltage for the servo valve yields

$$u_{Li} = \sqrt{\Delta p_r / (p_s - \text{sign}(Q_{Li}) P_{Li})} u_{\max} Q_{Li} / Q_r \tag{7}$$

where, u_{Li} is the control voltage, Q_r is the rated flow under the rated load pressure Δp_r and u_{\max} is the max control voltage. Defining the state variable as $x_i = [x_{i1}, x_{i2}, x_{i3}]^T = [F_{zi}, \dot{x}_{pi}, P_{Li}]^T$, the system state representation yields

$$\begin{cases} \dot{x}_{i1} = \theta_i x_{i2} - \theta_i \dot{x}_{pfi} + \Delta_i \\ \dot{x}_{i2} = \theta_{i1} x_{i3} - \theta_{i2} x_{i2} - \theta_{i3} x_{i1} + d_{hi} \\ \dot{x}_{i3} = -\theta_{i4} x_{i2} - \theta_{i5} x_{i3} + \theta_{i6} Q_{Li} \end{cases} \tag{8}$$

where, $\theta_i = k_f / (1 + \sin \gamma_i)$, $\theta_{i1} = A_p / m_i$, $\theta_{i2} = B_{pi} / m_i$, $\theta_{i3} = 1 / m_i$, $\theta_{i4} = 4A_p \beta_e / V_{ti}$, $\theta_{i5} = 4C_{tli} \beta_e / V_{ti}$, $\theta_{i6} = 4\beta_e / V_{ti}$.

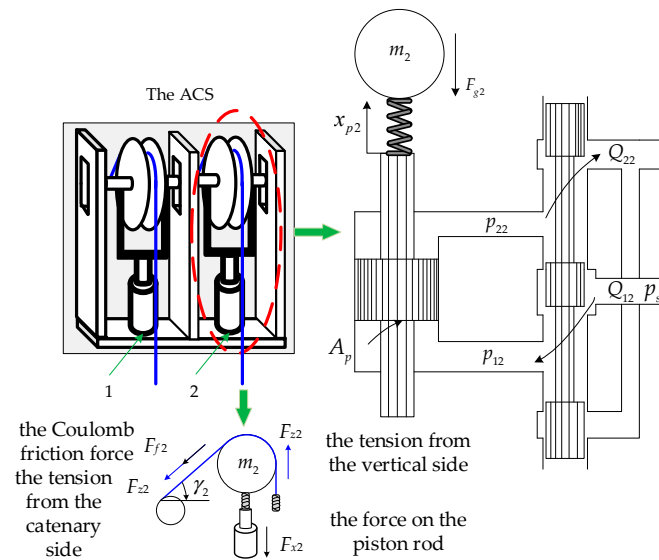


Figure 1. Schematic diagram of the ACS.

Assumption 1. Wire rope tensions F_{zi} and, its time derivatives \dot{F}_{zi} , \ddot{F}_{zi} and \ddot{F}_{zi} are all bounded.

Assumption 2. Disturbances Δ_i , d_{hi} and their first order time derivatives $\dot{\Delta}_i$ and \dot{d}_{hi} are varying slowly and bounded, i.e., $\dot{\Delta}_i \approx 0$, $\dot{d}_{hi} \approx 0$, $|\Delta_i| \leq \vartheta_i$, $|d_{hi}| \leq \zeta_i$, $|\dot{\Delta}_i| \leq v_i$ and $|\dot{d}_{hi}| \leq v_i$.

Remark 1. In this section, we describe a new model for the ACS of the hoisting system. (1) As shown in Equation (3), a differentiable tension model is established by choosing the tension derivative as one of the ACS’s state variables. Moreover, the Coulomb friction and coupled disturbances are specially considered in the model. The noncoupled disturbances mainly exist in the differentiable force model. (2) Coupled disturbances in the ACS are formulated in the differentiable speed model (4), which indicates that disturbances are delivered through vibrations in mechanical structures. With the state-space model of the ACS, the TDO, the CDO as well as the MDOBC will be developed in the next section.

3. Controller Design

3.1. Development of the TDO

Consider the following disturbance observer

$$\begin{cases} \dot{\hat{\Delta}}_i = \xi_i + p(x_{i1}, x_{i2}) \\ \dot{\xi}_i = -\frac{1}{\lambda_i}[\xi_i + p(x_{i1}, x_{i2})] + \frac{1}{\lambda_i}(-\theta_i x_{i2} + \theta_i x_{fpi}) \end{cases} \quad (9)$$

where, $p(x_{i1}, x_{i2})$ is a function that needs to be designed, λ_i is the control gain, ξ_i is an auxiliary variable. In order to make the TDO stable, the function $p(x_{i1}, x_{i2})$ and the control gain λ_i should satisfy $\dot{x}_{i1}/\lambda_i = \dot{p}(x_{i1}, x_{i2})$ [39,40]. Define the estimation error as $\tilde{\Delta}_i = \hat{\Delta}_i - \Delta_i$. The estimation error dynamics yields

$$\begin{aligned} \dot{\tilde{\Delta}}_i &= \dot{\hat{\Delta}}_i - \dot{\Delta}_i = \dot{\xi}_i + \dot{p}(x_{i1}, x_{i2}) - \dot{\Delta}_i \\ &= -\frac{1}{\lambda_i}[\xi_i + p(x_{i1}, x_{i2})] + \frac{1}{\lambda_i}(-\theta_i x_{i2} + \theta_i x_{fpi}) + \frac{1}{\lambda_i} \dot{x}_{i1} - 0 \\ &= -\frac{1}{\lambda_i}[\xi_i + p(x_{i1}, x_{i2})] + \frac{1}{\lambda_i}(\dot{x}_{i1} - \theta_i x_{i2} + \theta_i x_{fpi}) \\ &= -\frac{1}{\lambda_i} \hat{\Delta}_i + \frac{1}{\lambda_i} \Delta_i = -\frac{1}{\lambda_i} \tilde{\Delta}_i \end{aligned} \quad (10)$$

Therefore, the function $p(x_{i1}, x_{i2})$ can be designed as

$$p(x_{i1}, x_{i2}) = \frac{1}{\lambda_i} x_{i1}, \quad i = 1, 2. \quad (11)$$

With the result of Equation (11), the TDO for the ACS yields

$$\begin{cases} \hat{\Delta}_i = \zeta_i + \frac{1}{\lambda_i} x_{i1} \\ \dot{\zeta}_i = -\frac{1}{\lambda_i} \left[\zeta_i + \frac{1}{\lambda_i} x_{i1} \right] + \frac{1}{\lambda_i} \left(-\theta_i x_{i2} + \theta_i x_{fpi} \right) \end{cases} \quad (12)$$

The stability proof for the TDO is presented in Appendix A.

Remark 2. As is shown in Equations (3), (4) and (8), disturbances deriving from the Coulomb friction mainly appear in the first-order and second-order equations of the state space model. The section presents a TDO for estimating the disturbances in the first-order equation. The disturbances in the second-order equation will be estimated by the CDO in the next section.

3.2. Development of the CDO

The CDO for the ACS can be presented as [37]

$$\begin{bmatrix} \hat{d}_{h1} & \hat{d}_{h2} \end{bmatrix}^T = \mathbf{A} \begin{bmatrix} x_{12} - \hat{x}_{12} & x_{22} - \hat{x}_{22} \end{bmatrix}^T \quad (13)$$

where, \hat{d}_{hi} is the estimation value of d_{hi} , \hat{x}_{i2} is the estimation value of x_{i2} , \mathbf{A} is the control gain matrix of the CDO, $\mathbf{A} = [k_{d11}, k_{d12}; k_{d21}, k_{d22}]$ and, k_{d12} and k_{d21} are decoupling terms. Note that \mathbf{A} is a Hurwitz matrix and that it is dominated by its diagonal elements. Actually, \hat{x}_{i2} are estimation values of x_{i2} with the compensation from the CDO.

$$\begin{bmatrix} \dot{\hat{x}}_{12} \\ \dot{\hat{x}}_{22} \end{bmatrix} = \begin{bmatrix} -\theta_{13} & \theta_{11} & -\theta_{12} & 0 & 0 & 0 \\ 0 & 0 & 0 & -\theta_{23} & \theta_{21} & -\theta_{22} \end{bmatrix} \begin{bmatrix} x_{11} & 0 \\ x_{12} & 0 \\ x_{13} & 0 \\ 0 & x_{21} \\ 0 & x_{22} \\ 0 & x_{23} \end{bmatrix} + \begin{bmatrix} \hat{d}_{h1} \\ \hat{d}_{h2} \end{bmatrix} \quad (14)$$

The dynamics of the estimation value \hat{d}_{hi} yield

$$\begin{bmatrix} \dot{\hat{d}}_{h1} & \dot{\hat{d}}_{h2} \end{bmatrix}^T = \mathbf{A} \begin{bmatrix} \dot{x}_{12} - \dot{\hat{x}}_{12} & \dot{x}_{22} - \dot{\hat{x}}_{22} \end{bmatrix}^T \quad (15)$$

The estimation error dynamics of the CDO yield

$$\dot{\tilde{d}}_{hi} = -k_{dii} \tilde{d}_{hi} - \dots - k_{dii} \tilde{d}_{hi} + \dot{d}_{hi} \quad (16)$$

The stability analysis of the CDO is presented in Appendix A.

Remark 3. It can be seen that the coupled disturbances mainly derive from the Coulomb friction force and the external load force. By adjusting diagonal terms k_{d11} and k_{d22} in \mathbf{A} , the noncoupled disturbances in the differentiable speed model can be compensated. What's more, the coupled disturbances can be estimated simultaneously by the decoupling terms k_{d11} and k_{d22} in \mathbf{A} . With the estimation values from the CDO, both noncoupled and coupled disturbances can be compensated in the following controller.

3.3. Development of the MDOBC

Based on the state representation, the system tracking error can be presented as

$$\mathbf{e} = [e_{i1}, e_{i2}, e_{i3}], e_{i1} = x_{i1} - x_{ir}, e_{i2} = x_{i2} - \alpha_{i1}, e_{i3} = x_{i3} - \alpha_{i2}, i = 1, 2. \quad (17)$$

where, e_{i1} is the two-wire rope tension tracking errors, e_{i2} is the two displacement velocity tracking errors, e_{i3} is the two load pressure tracking errors and α_{i1} and α_{i2} , $i = 1, 2$. are the virtual control laws.

Theorem. *Considering the system state representation (8) and estimation values $\hat{\Delta}_i$ and \hat{d}_{hi} from the TDO and the CDO, there exists the following control law (18), which will guarantee that the system tracking error e enters into a bounded hypersphere ball H_r , $\forall t > 0$.*

$$\begin{cases} \alpha_{i1} = \left(-k_{i1}e_{i1} + \theta_i \dot{x}_{pfi} - \hat{\Delta}_i + \dot{x}_{ir} \right) / \theta_i \\ \alpha_{i2} = \left(-k_{i2}e_{i2} - \theta_i e_{i1} + \theta_{i2}x_{i2} + \theta_{i3}x_{i1} - \hat{d}_{hi} + \dot{\alpha}_{i1} \right) / \theta_{i1} \\ Q_{Li} = \left(-k_{i3}e_{i3} - \theta_{i1}e_{i2} + \theta_{i4}x_{i2} + \theta_{i5}x_{i3} + \dot{\alpha}_{i2} \right) / \theta_{i6} \end{cases}, i = 1, 2. \quad (18)$$

where the hypersphere ball H_r can be presented as

$$\begin{aligned} H_r = & - \sum_{i=1}^2 k_{i1} \left(e_{i1} - \frac{1}{2k_{i1}} \tilde{\Delta}_i \right)^2 - \sum_{i=1}^2 \left(\frac{1}{\lambda_i} - \frac{1}{4k_{i1}} \right) \tilde{\Delta}_i^2 \\ & - \sum_{i=1}^2 k_{i3} e_{i3}^2 - \sum_{i=1}^2 k_{i2} \left(e_{i2} + \frac{1}{2k_{i2}} \tilde{d}_{hi} \right)^2 - \sum_{i=1}^2 \delta_i \left[\tilde{d}_{hi} + \frac{1}{2\delta_i} \dot{d}_{hi} \right]^2 + \sum_{i=1}^2 \frac{v_i^2}{4\delta_i} \end{aligned}, i = 1, 2. \quad (19)$$

where, $\delta_i = k_{dii} - 1/4k_{i2}$. Therefore, if the control gains are properly selected as $k_{ij} > 0$ ($i = 1, 2, j = 1, 2, 3$), $k_{dii} > 1/4k_{i2}$ and $1/\lambda_i > 1/4k_{i1}$, the system tracking error e will enter into a bounded hypersphere ball H_r , $\forall t > 0$, and holds in H_r , $\forall t > t_0$. The closed-loop is bounded stable.

Proof. The N1HC backstepping iteration. Step 1-1: If the force dynamics in (8) and $\tilde{\Delta}_1 = \hat{\Delta}_1 - \Delta_1$ are substituted into $\dot{e}_{11} = \dot{x}_{11} - \dot{x}_{1r}$, the derivative \dot{e}_{11} yields

$$\dot{e}_{11} = \theta_1 x_{12} - \theta_1 \dot{x}_{pf1} + \hat{\Delta}_1 - \tilde{\Delta}_1 - \dot{x}_{1r}. \quad (20)$$

Define a Lyapunov function as $\chi_{11} = e_{11}^2/2 + \tilde{\Delta}_1^2/2$. With $e_{12} = x_{12} - \alpha_{11}$ in (17), one can derive $x_{12} = e_{12} + \alpha_{11}$. The derivative $\dot{\chi}_{11}$ can be presented as

$$\begin{aligned} \dot{\chi}_{11} &= e_{11} \dot{e}_{11} + \tilde{\Delta}_1 \dot{\tilde{\Delta}}_1 \\ &= e_{11} \left(\theta_1 x_{12} - \theta_1 \dot{x}_{pf1} + \hat{\Delta}_1 - \tilde{\Delta}_1 - \dot{x}_{1r} \right) + \tilde{\Delta}_1 \dot{\tilde{\Delta}}_1 \\ &= e_{11} \left(\theta_1 e_{12} + \theta_1 \alpha_{11} - \theta_1 \dot{x}_{pf1} + \hat{\Delta}_1 - \tilde{\Delta}_1 - \dot{x}_{1r} \right) + \tilde{\Delta}_1 \dot{\tilde{\Delta}}_1 \end{aligned}. \quad (21)$$

If the virtual control law α_{11} in (18) is substituted into (20), one can derive the following equation:

$$\dot{\chi}_{11} = -k_{11}e_{11}^2 + \theta_1 e_{11}e_{12} - e_{11}\tilde{\Delta}_1 - \tilde{\Delta}_1^2/\lambda_1. \quad (22)$$

Step 1-2: It can be seen that $\dot{\chi}_{11}$ (22) contains a cross-multiplying term $\theta_1 e_{11}e_{12}$; therefore, in order to eliminate it, define a Lyapunov function as

$$\chi_{12} = \chi_{11} + e_{12}^2/2 + \tilde{d}_{h1}^2/2. \quad (23)$$

If the speed dynamics in (8) and $d_{h1} = \hat{d}_{h1} - \tilde{d}_{h1}$ are substituted into $\dot{e}_{12} = \dot{x}_{12} - \dot{\alpha}_{11}$, the derivative \dot{e}_{12} yields

$$\dot{e}_{12} = \theta_{11}x_{13} - \theta_{12}x_{12} - \theta_{13}x_{11} + \hat{d}_{h1} - \tilde{d}_{h1} - \dot{\alpha}_{11}. \quad (24)$$

The time derivative of χ_{12} yields

$$\dot{\chi}_{12} = \dot{\chi}_{11} + e_{12}\dot{e}_{12} + \tilde{d}_{h1}\dot{\tilde{d}}_{h1}. \quad (25)$$

If $e_{13} = x_{13} - \alpha_{12}$ in (17), $\dot{\chi}_{11}$ in (22) and \tilde{d}_{hi} in (16) are substituted into (25), $\dot{\chi}_{12}$ can be further presented as

$$\begin{aligned} \dot{\chi}_{12} = & -k_{11}e_{11}^2 - \tilde{\Delta}_1^2/\lambda_1 + \theta_1e_{11}e_{12} + e_{11}\tilde{\Delta}_1 \\ & + e_{12}\left(\theta_{11}\alpha_{12} + \theta_{11}e_{13} - \theta_{12}x_{12} - \theta_{13}x_{11} + \dot{\hat{d}}_{h1} - \tilde{d}_{h1} - \dot{\alpha}_{11}\right) . \end{aligned} \quad (26)$$

$$-k_{d11}\tilde{d}_{h1}^2 - k_{d12}\tilde{d}_{h1}\tilde{d}_{h2} + \tilde{d}_{h1}\dot{\hat{d}}_{h1}$$

If the virtual control law α_{12} in (17) is substituted into $\dot{\chi}_{12}$, one can derive the following equation.

$$\begin{aligned} \dot{\chi}_{12} = & -k_{11}e_{11}^2 - \tilde{\Delta}_1^2/\lambda_1 + \theta_{11}e_{12}e_{13} - k_{12}e_{12}^2 - e_{12}\tilde{d}_{h1} \\ & + e_{11}\tilde{\Delta}_1 - k_{d11}\tilde{d}_{h1}^2 - k_{d12}\tilde{d}_{h1}\tilde{d}_{h2} - \tilde{d}_{h1}\dot{\hat{d}}_{h1} . \end{aligned} \quad (27)$$

Step 1-3: The cross-multiplying term $\theta_{11}e_{12}e_{13}$ in $\dot{\chi}_{12}$ (27) can be eliminated by defining a Lyapunov function as

$$\chi_{13} = \chi_{12} + e_{13}^2/2. \quad (28)$$

With the load pressure dynamics in (8) and $e_{13} = x_{13} - \alpha_{12}$ in (17), the time derivative of e_{13} can be presented as

$$\dot{e}_{13} = -\theta_{14}x_{22} - \theta_{15}x_{23} + \theta_{16}Q_{L1} - \dot{\alpha}_{12}. \quad (29)$$

Therefore, the derivative $\dot{\chi}_{13}$ yields

$$\begin{aligned} \dot{\chi}_{13} = & \dot{\chi}_{12} + e_{13}\dot{e}_{13} \\ = & -k_{11}e_{11}^2 - \tilde{\Delta}_1^2/\lambda_1 + e_{11}\tilde{\Delta}_1 + \theta_{11}e_{12}e_{13} - k_{12}e_{12}^2 \\ & - e_{12}\tilde{d}_{h1} - k_{d11}\tilde{d}_{h1}^2 - k_{d12}\tilde{d}_{h1}\tilde{d}_{h2} - \tilde{d}_{h1}\dot{\hat{d}}_{h1} + e_{13}(-\theta_{14}x_{22} - \theta_{15}x_{23} + \theta_{16}Q_{L1} - \dot{\alpha}_{12}) \end{aligned} . \quad (30)$$

With the real control law Q_{L1} in (18), $\dot{\chi}_{13}$ can be rewritten as

$$\begin{aligned} \dot{\chi}_{13} = & -k_{11}e_{11}^2 - \tilde{\Delta}_1^2/\lambda_1 + e_{11}\tilde{\Delta}_1 - k_{12}e_{12}^2 - e_{12}\tilde{d}_{h1} - k_{d11}\tilde{d}_{h1}^2 - k_{13}e_{13}^2 - k_{d12}\tilde{d}_{h1}\tilde{d}_{h2} + \tilde{d}_{h1}\dot{\hat{d}}_{h1} \\ = & -k_{11}\left(e_{11}^2 - \frac{e_{11}\tilde{\Delta}_1}{k_{11}}\right) - \frac{\tilde{\Delta}_1^2}{\lambda_1} - k_{12}\left(e_{12}^2 + \frac{e_{12}\tilde{d}_{h1}}{k_{12}}\right) - k_{d11}\tilde{d}_{h1}^2 - \tilde{d}_{h1}\dot{\hat{d}}_{h1} - k_{13}e_{13}^2 - k_{d12}\tilde{d}_{h1}\tilde{d}_{h2} \\ = & -k_{11}\left(e_{11} - \frac{1}{2k_{11}}\tilde{\Delta}_1\right)^2 - \frac{\tilde{\Delta}_1^2}{\lambda_1} + \frac{1}{4k_{11}}\tilde{\Delta}_1^2 - k_{12}\left(e_{12} + \frac{\tilde{d}_{h1}}{2k_{12}}\right)^2 \\ & + \frac{\tilde{d}_{h1}^2}{4k_{12}} - k_{d11}\tilde{d}_{h1}^2 + \tilde{d}_{h1}\dot{\hat{d}}_{h1} - k_{13}e_{13}^2 - k_{d12}\tilde{d}_{h1}\tilde{d}_{h2} \\ = & -k_{11}\left(e_{11} - \frac{1}{2k_{11}}\tilde{\Delta}_1\right)^2 - \left(\frac{1}{\lambda_1} - \frac{1}{4k_{11}}\right)\tilde{\Delta}_1^2 - k_{12}\left(e_{12} + \frac{\tilde{d}_{h1}}{2k_{12}}\right)^2 \\ & - \left(k_{d11} - \frac{1}{4k_{12}}\right)\left[\tilde{d}_{h1} - \frac{1}{2\left(k_{d11} - \frac{1}{4k_{12}}\right)}\dot{\hat{d}}_{h1}\right]^2 + \frac{1}{4\left(k_{d11} - \frac{1}{4k_{12}}\right)}\dot{\hat{d}}_{h1}^2 - k_{13}e_{13}^2 - k_{d12}\tilde{d}_{h1}\tilde{d}_{h2} \\ = & -k_{11}\left(e_{11} - \frac{1}{2k_{11}}\tilde{\Delta}_1\right)^2 - \left(\frac{1}{\lambda_1} - \frac{1}{4k_{11}}\right)\tilde{\Delta}_1^2 - k_{13}e_{13}^2 \\ & - k_{12}\left(e_{12} + \frac{1}{2k_{12}}\tilde{d}_{h1}\right)^2 - \delta_1\left[\tilde{d}_{h1} - \frac{1}{2\delta_1}\dot{\hat{d}}_{h1}\right]^2 + \frac{\dot{\hat{d}}_{h1}^2}{4\delta_1} - k_{d12}\tilde{d}_{h1}\tilde{d}_{h2} \end{aligned} . \quad (31)$$

Remark 4. Note that the uncertain term $k_{d12}\tilde{d}_{h1}\tilde{d}_{h2}$ contains a disturbance \tilde{d}_{h2} from the N2HC. Therefore, one can eliminate it in the following N2HC backstepping iteration.

The N2HC backstepping iteration. Step 2-1: Define the following Lyapunov function as

$$\chi_{21} = e_{21}^2/2 + \tilde{\Delta}_2^2/2. \quad (32)$$

If the force dynamics in (8) and $\tilde{\Delta}_2 = \hat{\Delta}_2 - \Delta_2$ are substituted into $\dot{e}_{21} = \dot{x}_{21} - \dot{x}_{2r}$, the derivative \dot{e}_{21} yields

$$\dot{e}_{21} = \theta_2x_{22} - \theta_2\dot{x}_{pf2} + \hat{\Delta}_2 - \tilde{\Delta}_2 - \dot{x}_{2r}. \quad (33)$$

Therefore, the derivative $\dot{\chi}_{21}$ yields

$$\begin{aligned}\dot{\chi}_{21} &= e_{21}\dot{e}_{21} + \tilde{\Delta}_2\dot{\tilde{\Delta}}_2 \\ &= e_{21}\left(\theta_2 e_{22} + \theta_2 \alpha_{21} - \theta_2 \dot{x}_{pf2} + \hat{\Delta}_2 - \tilde{\Delta}_2 - \dot{x}_{2r}\right) + \tilde{\Delta}_2\dot{\tilde{\Delta}}_2.\end{aligned}\quad (34)$$

With the virtual control law α_{21} in (18), therefore,

$$\dot{\chi}_{21} = -k_{21}e_{21}^2 + \theta_2 e_{21}e_{22} - e_{21}\tilde{\Delta}_2 - \tilde{\Delta}_2^2/\lambda_2. \quad (35)$$

Step 2-2: It can be seen that $\dot{\chi}_{21}$ contains a cross-multiplying term $\theta_2 e_{21}e_{22}$. Define a Lyapunov function as

$$\chi_{22} = \chi_{21} + e_{22}^2/2 + \tilde{d}_{h2}^2/2. \quad (36)$$

If the speed dynamics in (8) and $d_{h2} = \hat{d}_{h2} - \tilde{d}_{h2}$ are substituted into $\dot{e}_{22} = \dot{x}_{22} - \dot{\alpha}_{21}$, one can derive \dot{e}_{22} yielding

$$\dot{e}_{22} = \theta_{21}x_{23} - \theta_{22}x_{22} - \theta_{23}x_{21} + \hat{d}_{h2} - \tilde{d}_{h2} - \dot{\alpha}_{21}. \quad (37)$$

Further, the time derivative of χ_{22} yields

$$\begin{aligned}\dot{\chi}_{22} &= \dot{\chi}_{21} + e_{22}\dot{e}_{22} + \tilde{d}_{h2}\dot{\tilde{d}}_{h2} \\ &= -k_{21}e_{21}^2 - \tilde{\Delta}_2^2/\lambda_2 + \theta_2 e_{21}e_{22} + e_{21}\tilde{\Delta}_2 - k_{d22}\tilde{d}_{h2}^2 + \tilde{d}_{h2}\dot{d}_{h2} - k_{d21}\tilde{d}_{h1}\tilde{d}_{h2} \\ &\quad + e_{22}\left(\theta_{21}\alpha_{22} + \theta_{21}e_{23} - \theta_{22}x_{22} - \theta_{23}x_{21} + \hat{d}_{h2} - \tilde{d}_{h2} - \dot{\alpha}_{21}\right)\end{aligned}\quad (38)$$

With the virtual control law α_{22} in (18), $\dot{\chi}_{22}$ yields

$$\dot{\chi}_{22} = -k_{21}e_{21}^2 - \tilde{\Delta}_2^2/\lambda_2 + \theta_{21}e_{22}e_{23} - e_{22}\tilde{d}_{h2} + e_{21}\tilde{\Delta}_2 - k_{d21}\tilde{d}_{h1}\tilde{d}_{h2} - k_{d22}\tilde{d}_{h2}^2 + \tilde{d}_{h2}\dot{d}_{h2}. \quad (39)$$

Step 2-3: It can be seen that $\dot{\chi}_{22}$ still contains $\theta_{21}e_{22}e_{23}$; therefore, define the following Lyapunov function as

$$\chi_{23} = \chi_{22} + e_{23}^2/2. \quad (40)$$

If the load pressure dynamics in (8) are substituted into $\dot{e}_{23} = \dot{x}_{23} - \dot{\alpha}_{22}$, one can derive \dot{e}_{23} yielding

$$\dot{e}_{23} = -\theta_{24}x_{22} - \theta_{25}x_{23} + \theta_{26}Q_{L2} - \dot{\alpha}_{22} \quad (41)$$

With Equation (41), the derivative $\dot{\chi}_{23}$ yields

$$\begin{aligned}\dot{\chi}_{23} &= \dot{\chi}_{22} + e_{23}\dot{e}_{23} \\ &= -k_{21}e_{21}^2 - \frac{1}{\lambda_2}\tilde{\Delta}_2^2 + \theta_{21}e_{22}e_{23} - e_{22}\tilde{d}_{h2} + e_{21}\tilde{\Delta}_2 - k_{d21}\tilde{d}_{h1}\tilde{d}_{h2} - k_{d22}\tilde{d}_{h2}^2 + \tilde{d}_{h2}\dot{d}_{h2} + e_{23}\dot{e}_{23} \\ &= -k_{21}e_{21}^2 - \tilde{\Delta}_2^2/\lambda_2 + e_{21}\tilde{\Delta}_2 + \theta_{21}e_{22}e_{23} - k_{22}e_{22}^2 - e_{22}\tilde{d}_{h2} - k_{d22}\tilde{d}_{h2}^2 \\ &\quad - k_{d21}\tilde{d}_{h1}\tilde{d}_{h2} + \tilde{d}_{h2}\dot{d}_{h2} + e_{23}\left[-\theta_{24}x_{22} - \theta_{25}x_{23} + \theta_{26}Q_{L2} - \dot{\alpha}_{22}\right]\end{aligned}\quad (42)$$

With the real control law Q_{L2} in (18), $\dot{\chi}_{23}$ yields

$$\begin{aligned}
 \dot{\chi}_{23} &= -k_{21}e_{21}^2 - \tilde{\Delta}_2^2/\lambda_2 + e_{21}\tilde{\Delta}_2 - k_{22}e_{22}^2 - e_{22}\tilde{d}_{h2} - k_{d22}\tilde{d}_{h2}^2 - k_{23}e_{23}^2 - k_{d21}\tilde{d}_{h1}\tilde{d}_{h2} + \tilde{d}_{h2}\dot{d}_{h2} \\
 &= -k_{21}\left(e_{21} - \frac{1}{2k_{21}}\tilde{\Delta}_2\right)^2 + \frac{\tilde{\Delta}_2^2}{4k_{21}} - \frac{\tilde{\Delta}_2^2}{\lambda_2} - k_{22}\left(e_{22} + \frac{1}{2k_{22}}\tilde{d}_{h2}\right)^2 + \frac{1}{4k_{22}}\tilde{d}_{h2}^2 - k_{d22}\tilde{d}_{h2}^2 \\
 &\quad + \tilde{d}_{h2}\dot{d}_{h2} - k_{23}e_{23}^2 - k_{d21}\tilde{d}_{h1}\tilde{d}_{h2} \\
 &= -k_{21}\left(e_{21} - \frac{1}{2k_{21}}\tilde{\Delta}_2\right)^2 - \left(\frac{1}{\lambda_2} - \frac{1}{4k_{21}}\right)\tilde{\Delta}_2^2 - k_{22}\left(e_{22} + \frac{1}{2k_{22}}\tilde{d}_{h2}\right)^2 - \left(k_{d22} - \frac{1}{4k_{22}}\right)\tilde{d}_{h2}^2 \\
 &\quad + \tilde{d}_{h2}\dot{d}_{h2} - k_{23}e_{23}^2 - k_{d21}\tilde{d}_{h1}\tilde{d}_{h2} \\
 &= -k_{21}\left(e_{21} - \frac{1}{2k_{21}}\tilde{\Delta}_2\right)^2 - \left(\frac{1}{\lambda_2} - \frac{1}{4k_{21}}\right)\tilde{\Delta}_2^2 - k_{22}\left(e_{22} + \frac{1}{2k_{22}}\tilde{d}_{h2}\right)^2 \\
 &\quad - \left(k_{d22} - \frac{1}{4k_{22}}\right)\left[\tilde{d}_{h2} - \frac{1}{\left(k_{d22} - \frac{1}{4k_{22}}\right)}\dot{d}_{h2}\right]^2 + \frac{1}{4\left(k_{d22} - \frac{1}{4k_{22}}\right)}\dot{d}_{h2}^2 - k_{23}e_{23}^2 - k_{d21}\tilde{d}_{h1}\tilde{d}_{h2} \\
 &= -k_{21}\left(e_{21} - \frac{1}{2k_{21}}\tilde{\Delta}_2\right)^2 - \left(\frac{1}{\lambda_2} - \frac{1}{4k_{21}}\right)\tilde{\Delta}_2^2 - k_{23}e_{23}^2 \\
 &\quad - k_{22}\left(e_{22} + \frac{1}{2k_{22}}\tilde{d}_{h2}\right)^2 - \delta_2\left[\tilde{d}_{h2} - \frac{1}{2\delta_2}\dot{d}_{h2}\right]^2 + \frac{\dot{d}_{h2}^2}{4\delta_2} - k_{d21}\tilde{d}_{h1}\tilde{d}_{h2}
 \end{aligned} \tag{43}$$

Note that the term $k_{d21}\tilde{d}_{h1}\tilde{d}_{h2}$ in $\dot{\chi}_{23}$ is employed to eliminate the uncertain term $k_{d21}\tilde{d}_{h1}\tilde{d}_{h2}$ in $\dot{\chi}_{13}$. Since the matrix A is a Hurwitz matrix, $k_{d12} = -k_{d21}$ and $k_{d21}\tilde{d}_{h1}\tilde{d}_{h2} + k_{d21}\dot{d}_{h1}\dot{d}_{h2} = 0$. Therefore, if the derivative $\dot{\chi}_{13}$ (30) is substituted into $\dot{\chi}_{23}$ (43), one can obtain the following formula.

$$\begin{aligned}
 \dot{\chi}_{23} &= -\sum_{i=1}^2 k_{i1}\left(e_{i1} - \frac{1}{2k_{i1}}\tilde{\Delta}_i\right)^2 - \sum_{i=1}^2 \left(\frac{1}{\lambda_i} - \frac{1}{4k_{i1}}\right)\tilde{\Delta}_i^2 - \sum_{i=1}^2 k_{i3}e_{i3}^2 - \sum_{i=1}^2 k_{i2}\left(e_{i2} + \frac{1}{2k_{i2}}\tilde{d}_{hi}\right)^2 \\
 &\quad - \sum_{i=1}^2 \delta_i\left[\tilde{d}_{hi} - \frac{1}{2\delta_i}\dot{d}_{hi}\right]^2 + \sum_{i=1}^2 \frac{\dot{d}_{hi}^2}{4\delta_i} - \underbrace{k_{d21}\tilde{d}_{h1}\tilde{d}_{h2} - k_{d21}\tilde{d}_{h1}\tilde{d}_{h2}}_{=0}
 \end{aligned} \tag{44}$$

Since the disturbances are bounded, $|\dot{d}_{hi}| \leq v_i$, further,

$$\begin{aligned}
 \dot{\chi}_{23} &\leq -\sum_{i=1}^2 k_{i1}\left(e_{i1} - \frac{1}{2k_{i1}}\tilde{\Delta}_i\right)^2 - \sum_{i=1}^2 \left(\frac{1}{\lambda_i} - \frac{1}{4k_{i1}}\right)\tilde{\Delta}_i^2 - \sum_{i=1}^2 k_{i3}e_{i3}^2 \\
 &\quad - \sum_{i=1}^2 k_{i2}\left(e_{i2} + \frac{1}{2k_{i2}}\tilde{d}_{hi}\right)^2 - \sum_{i=1}^2 \delta_i\left[\tilde{d}_{hi} - \frac{1}{2\delta_i}\dot{d}_{hi}\right]^2 + \sum_{i=1}^2 \frac{v_i^2}{4\delta_i}
 \end{aligned} \tag{45}$$

There is only one positive definite term $\sum v_i^2/4\delta_i, i = 1, 2$, in $\dot{\chi}_{23}$, and other terms in $\dot{\chi}_{23}$ are all negative definite. Therefore, if sufficient control gains are properly chosen, $\dot{\chi}_{23}$ can be guaranteed to be negative definite and the stability of the MDOBC can be guaranteed. □

Remark 5. The proof for the MDOBC is conducted on the N1HC and the N2HC separately through the backstepping iteration technique. By employing the backstepping iteration with proposed virtual control laws in (18), we eliminate the cross-multiplying terms in the corresponding time derivative of a proper Lyapunov function for each subsystem; subsequently, we derive the final Lyapunov functions for the N1HC and the N2HC, thus the stability of the closed loop is proven with proposed real control laws in (18). Since the coupled disturbances exist in the ACS, the term $k_{d12}\tilde{d}_{h1}\tilde{d}_{h2}$ in $\dot{\chi}_{13}$ should be eliminated by $k_{d21}\tilde{d}_{h1}\tilde{d}_{h2}$ in $\dot{\chi}_{23}$. Therefore, we substitute $\dot{\chi}_{13}$ into $\dot{\chi}_{23}$ to complete the stability proof for the MDOBC.

Remark 6. Since there are two Coulomb friction forces between two wire ropes and two moveable head sheaves, and the coupled disturbances will degrade the performance of the ACS, a TDO and a CDO are consequently designed to make online estimates of the disturbances and compensate for them. With those estimation values, a MDOBC is designed to coordinate two wire rope tensions. The coupled elements in the time derivative of $\dot{\chi}_{23}$ are eliminated since the CDO control gain matrix A is a Hurwitz matrix.

Remak 7. According to Assumption 2, disturbances d_{hi} vary slowly. Therefore, v_i should be a bounded small value, which indicates that other negative terms can hold $\dot{\chi}_{23} \leq 0$. To summarize the above statement, the MDOBC is stable.

4. Comparative Experimental Study

4.1. The Experimental Test Rig

Figure 2 presents the hoisting system’s experimental test rig. No. 1 and No. 2 denote the No. 1 and the No. 2 wire ropes, as well as their corresponding movable head sheaves, hydraulic cylinders, and winding drums. The mechanical construction is welded on the lower platform. The conveyance with four ears will be hoisted or lowered through four flexible guides, the two ends of which are fastened to the lower and the upper platforms, respectively. Two drums are secured to the upper platform by several screw bolts. Two hydraulic cylinders are positioned vertically so that they can push or pull two movable head sheaves in two stiff guide rails up or down. As a result, the tensions of the two wire ropes will be coordinated to reduce the tension difference. Two winding drums will hoist or lower the conveyance in accordance with the reference six-stage hoisting velocity, which forms a closed-loop with two corresponding encoders. Table 1 shows the key structural parameters of the experimental test rig. The key hydraulic parameters are presented in Table 2.

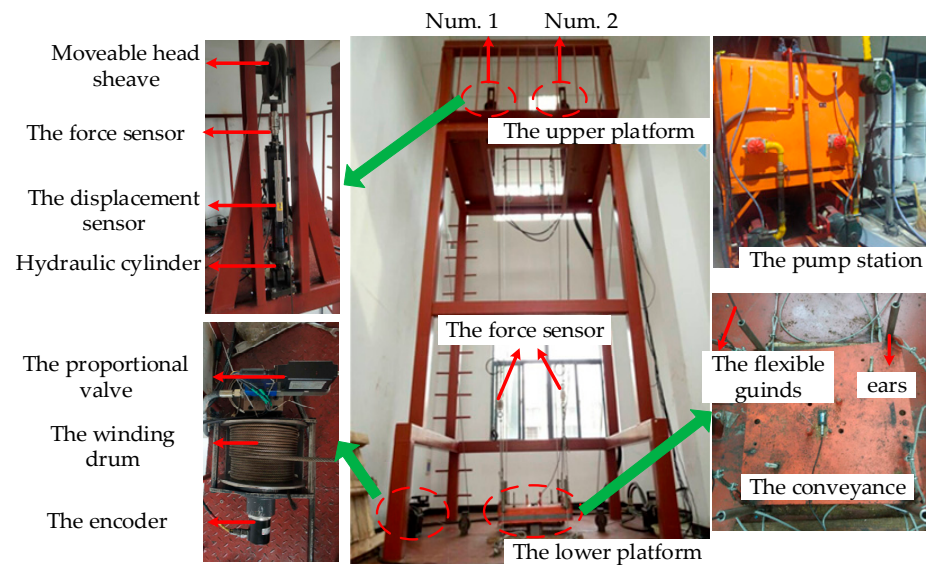


Figure 2. The experimental test rig.

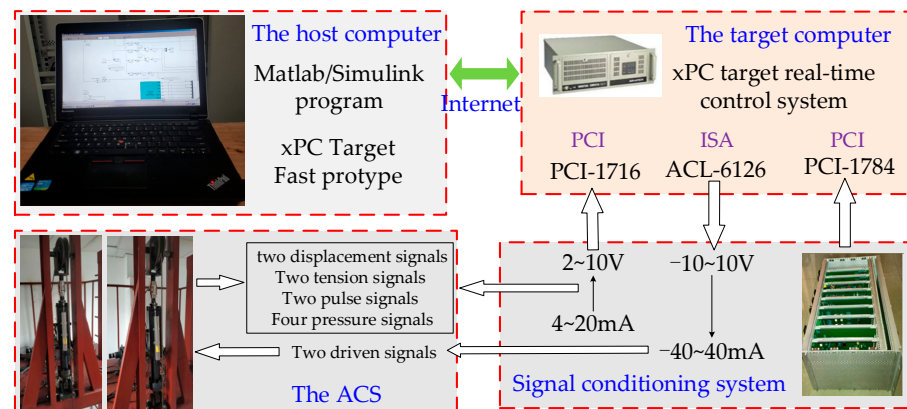
Table 1. Key structural parameters of the hoisting system.

Parameters	Values	Parameters	Values
Hoisting height	4.5 m	Width	3.4 m
Whole height	7 m	Length	4.4 m
Diameter of head sheave	0.5 m	Dimensions of the conveyance	0.375 × 0.375 × 0.125 m
Hoisting weight	200 Kg	Diameter of two winding drum	0.4 m

Table 2. Key hydraulic parameters of the hoisting system.

Parameters	Values/Unit	Parameters	Values/Unit
A_p	$1.88 \times 10^{-3} / \text{m}^2$	V_{ti}	$0.38 \times 10^{-3} \text{ m}^3$
m_i	110/Kg	u_{\max}	10 V
ΔP_r	21 MPa	P_s	$15 \times 10^6 \text{ Pa}$
B_{pi}	25,000 N/(m/s)	Q_r	30 L/min
C_{tli}	$6.9 \times 10^{-13} \text{ m}^3/\text{s}/\text{Pa}$	β_e	$6.9 \times 10^8 \text{ Pa}$

Figure 3 presents the real control system. The basic hardware of the real control system mainly consists of a host computer, a target computer, a signal conditioning system, and a sensor measurement system. Control algorithms written in Simulink will be converted into Visual C language and then delivered to the target computer through the Internet with the xPC Target fast prototyping technology. During the hoisting or the lowering stage, the PCI-1716 board will acquire two tension signals, two displacement signals, and four load pressure signals, which will be optimized by the signal conditioning system from 4–20 mA to 2–10 V. Two control signals for two proportional valves and two electro-hydraulic servo valves will be transformed from $\pm 10 \text{ V}$ to $\pm 40 \text{ mA}$ by the signal conditioning system and then conducted on two winding drums and two hydraulic cylinders. The sampling time of the real-time control system is 1 ms.

**Figure 3.** The real control system of the hoisting system.

4.2. Comparative Experimental Results

In the experimental study, a six-stage hoisting velocity signal in Figure 4 is employed and a $[\text{m}/\text{s}^2]$ denotes the acceleration in the hoisting phase or the lowering phase. The following six cases are considered. Note that all figures present two wire rope tensions with the black line denoting the No. 1 wire rope tension and the red line denoting the No. 2 wire rope tension.

- No controller: Without any A controller, wire rope tensions are presented in Figure 5.
- The PI controller: The PI controller can be expressed as $u_{Li} = K_{pi} \times e + K_{Ii} \Sigma e$. e denotes the tension tracking error. Control gains are selected as $K_{pi} = 0.012$ and $K_{Ii} = 0.05$. The experimental results are presented in Figure 6;
- The BC: With estimation values from the TDO and the CDO being defined as zero, the BC controller is conducted on the ACS. Control gains are selected as $k_{i1} = 3000$, $k_{i2} = 1000$, $k_{i3} = 1200$. The experimental results are presented in Figure 7;
- The TDO based BC: With estimation values from the CDO are defined as zeros, the TDO based BC is conducted on the ACS. Control gains are selected as $\lambda_i = 0.1$, $k_{i1} = 3000$, $k_{i2} = 1000$, $k_{i3} = 1200$. Figure 8 presents the experimental results;
- The CDO based BC: With estimation values from the TDO are defined as zeros, the CDO based BC is conducted on the ACS. Control gains are selected as $k_{d11} = 20$,

$k_{d12} = 0.1, k_{d21} = 0.1, k_{d22} = 20, k_{i1} = 3000, k_{i2} = 1000, k_{i3} = 1200$. The experimental results are presented in Figure 9;

- vi. The MDOBC: With the state representation, the MDOBC is designed and conducted on the ACS. Control gains are selected as $\lambda_i = 0.1, k_{d11} = 20, k_{d12} = 0.1, k_{d21} = 0.1, k_{d22} = 20, k_{i1} = 3000, k_{i2} = 1000, k_{i3} = 1200$. The corresponding experimental results are presented in Figure 10.

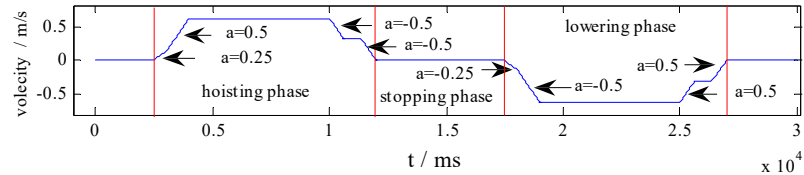


Figure 4. The six-stage velocity hoisting signal.

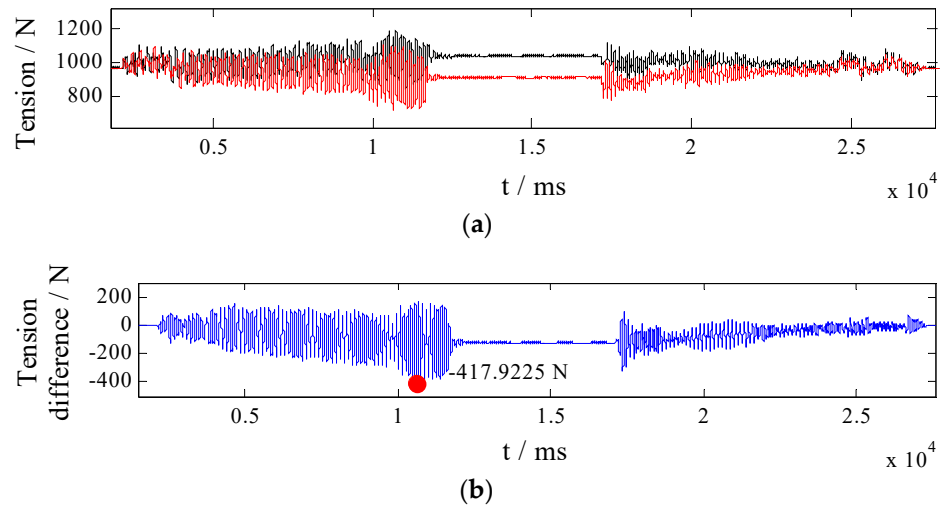


Figure 5. Two wire rope tensions without any A controller: (a) two wire rope tensions; (b) the tension difference.

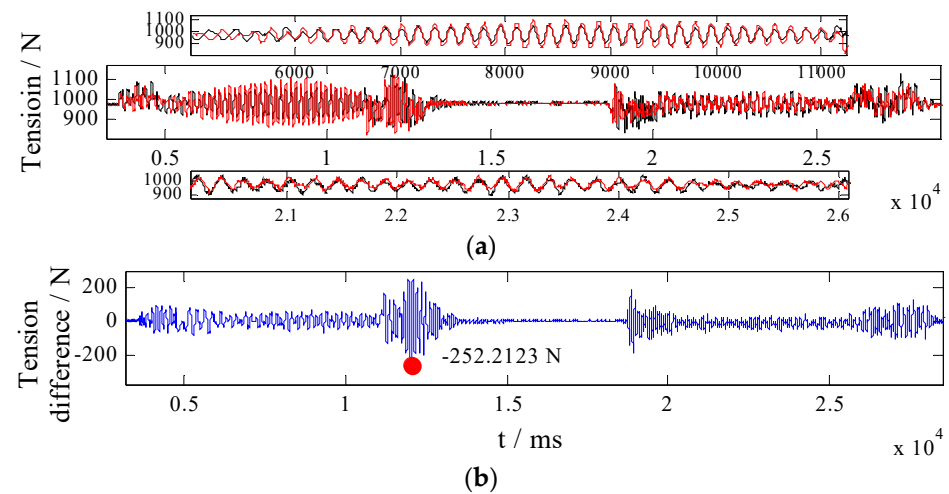


Figure 6. Two wire rope tensions with the PI controller: (a) two wire rope tensions; (b) the tension difference.

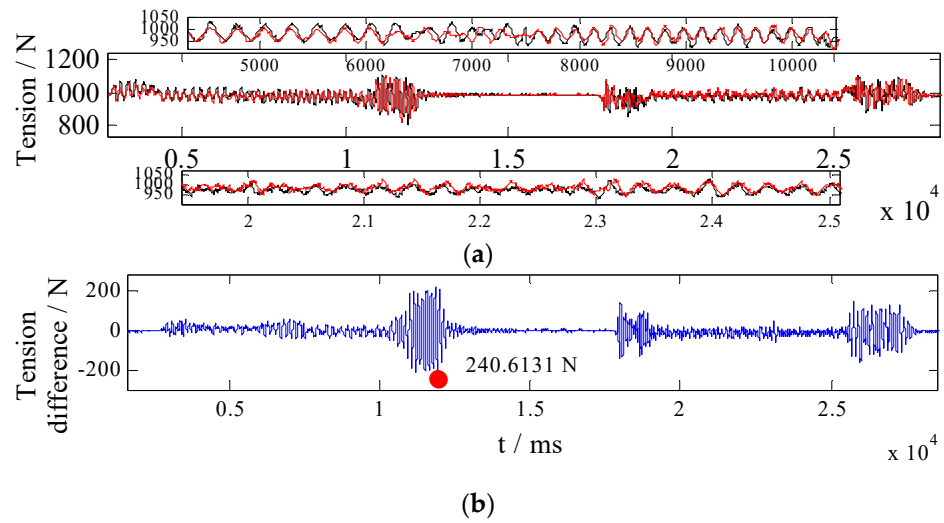


Figure 7. Two wire rope tensions with the BC controller: (a) two wire rope tensions; (b) the tension difference.

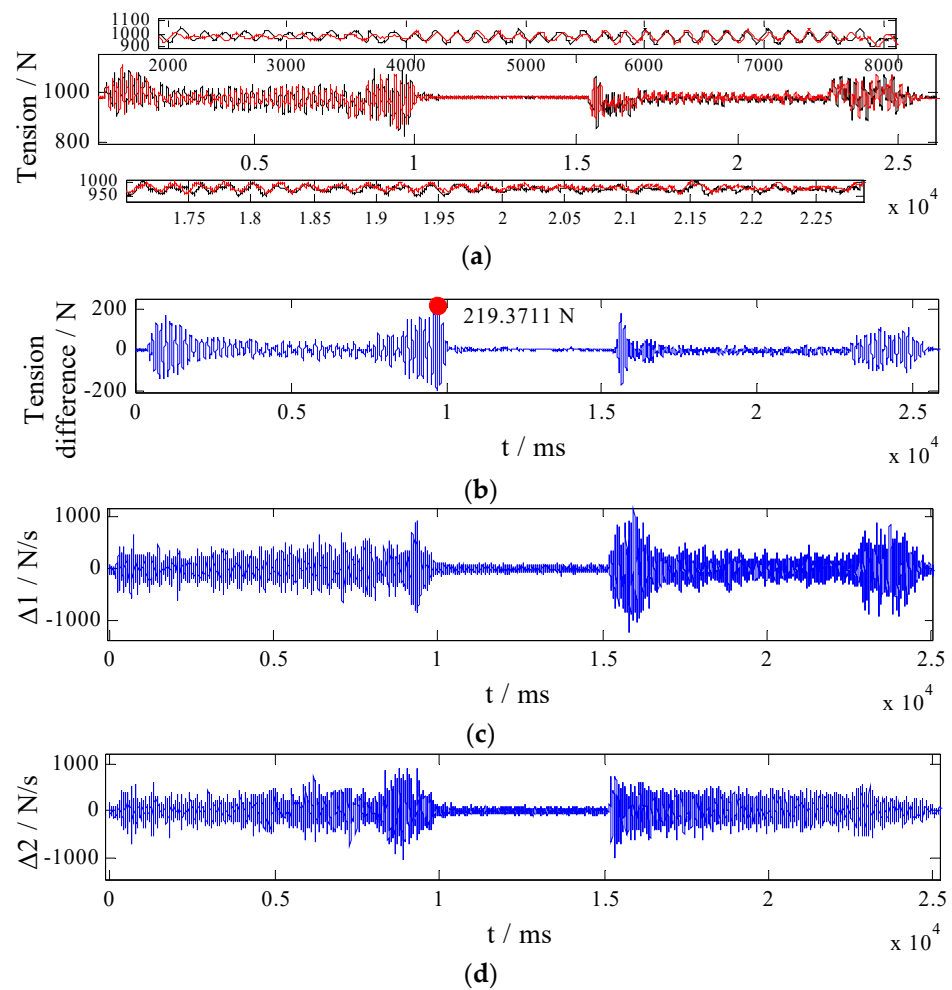


Figure 8. Two wire rope tensions with the TDO based BC controller: (a) two wire rope tensions; (b) the tension difference; (c) the estimation values of Δ_1 ; and (d) the estimation values of Δ_2 .

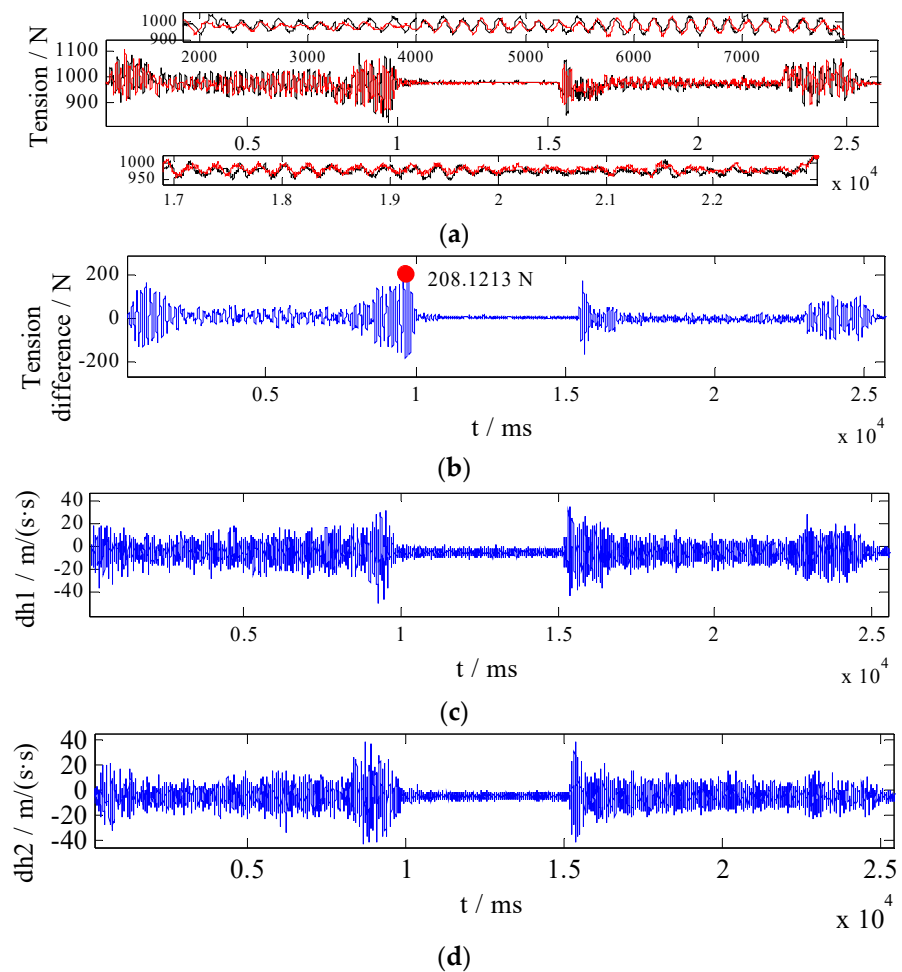


Figure 9. Two wire rope tensions with the CDO based BC controller: (a) two wire rope tensions; (b) the tension difference; (c) the estimation values of d_{h1} ; (d) the estimation values of d_{h2} .

The root mean square error (RMSE), employed to illustrate the performance of six controllers, yields

$$\text{RMSE} = \sqrt{\sum_i^n (R_{in,i} - R_{out,i})^2 / n}. \quad (46)$$

where $R_{in,i}$ denotes the reference signal, $R_{out,i}$ denotes the feedback signal from the displacement sensor, and n denotes the length of the signal. The RMSE results are presented in Table 3.

Table 3. The peak error and the RMSE.

Controllers	Peak Error/N	RMSE/N
Without any A controller	417.9225	106.5372
The PI controller	252.2123	38.1489
The BC	240.6131	37.5700
The TDO based BC	219.3711	32.7556
The CDO based BC	208.1213	30.7174
The proposed controller	190.2951	28.2601

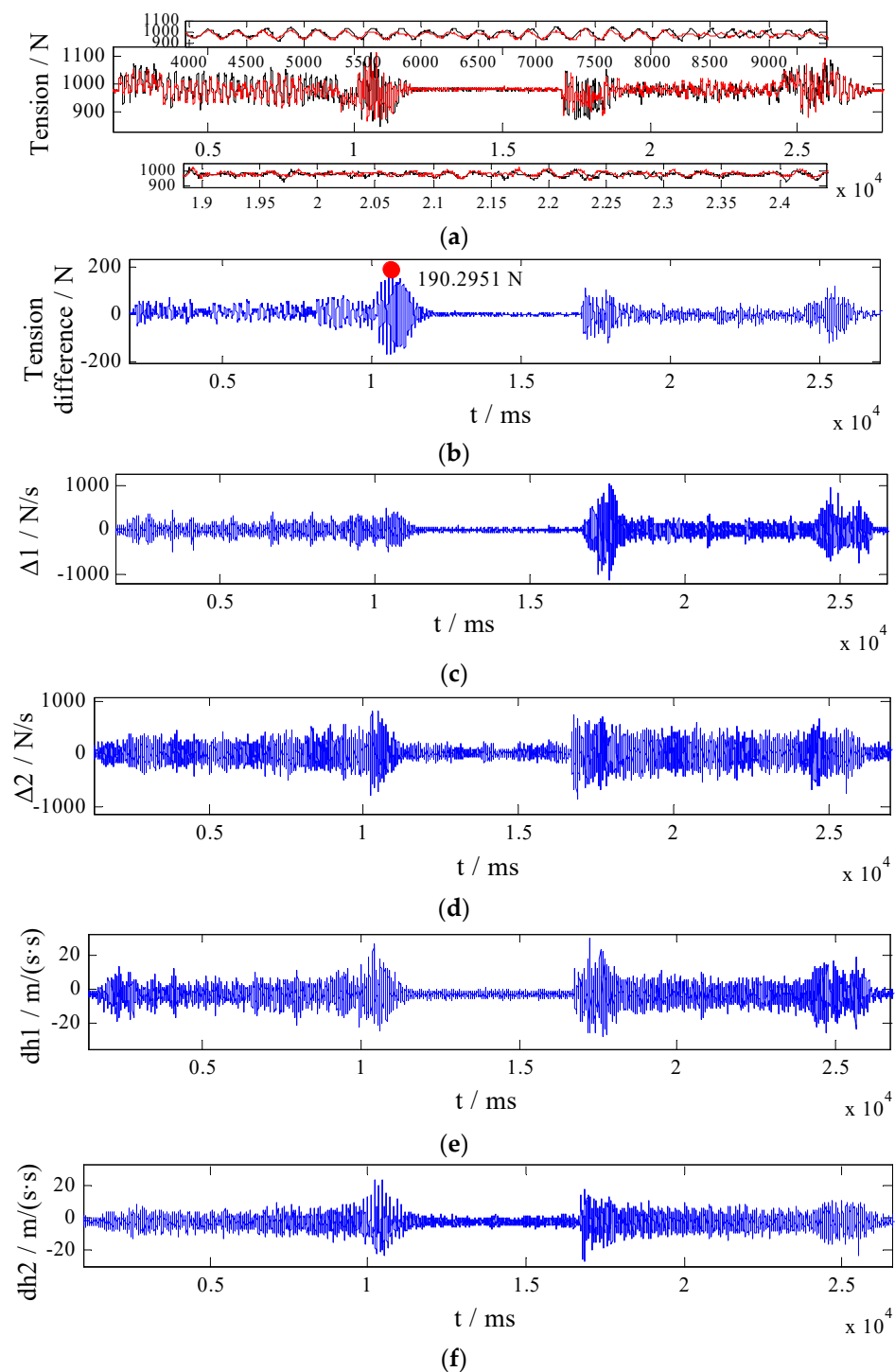


Figure 10. Two wire rope tensions with the proposed controller: (a) two wire rope tensions; (b) the tension difference; (c) the estimation values of Δ_1 ; (d) the estimation values of Δ_2 ; (e) the estimation values of d_{h1} ; and (f) the estimation values of d_{h2} .

As illustrated in Figure 5, without any A controller, the tension difference gradually increases in the hoisting stage, then approaches a predetermined value in the stopping stage, and then gradually decreases in the lowering stage. It is obvious that if no controller is utilized, the tension difference is significant. According to Figure 6, when the PI controller is employed, two wire rope tensions are essentially constant; nevertheless, its performance can be improved. Figure 7 presents two tensions of the BC. The vibrations of two wire ropes are decreased, and the performance is superior to that of the PI controller. Due to the

complicated disturbances, two tensions are discordant during some time in the hoisting stage or the lowering stage. It can be seen in Figures 8 and 9 that both the TDO based BC and the CDO based BC improve the coordination of two wire ropes. Two tensions with the MDOBC are presented in Figure 10. It can be concluded that the MDOBC can coordinate two wire rope tensions, and the vibrations of two wire ropes are further decreased. Table 3 shows the peak error and the RMSE. One can derive that without any a controller (417.9225 N) > with the PI controller (252.2123 N) > with the BC (240.6131 N) > with the TDO based BC (219.3711 N) > with the CDO based BC (208.1213 N) > with the MDOBC (190.2951 N). The tension difference is reduced from 252.2123 N with the PI controller to 190.2951 N with the MDOBC. The load balance can be further guaranteed so that the wear and tear of the wire ropes will be decreased. From the RMSE analysis, one can derive that without any A controller (106.5372) > the PI controller (38.1489) > the BC (37.5700) > the TDO based BC (32.7556) > the CDO based BC (30.7174) > the MDOBC (28.2601). The RMSE of the tension difference is reduced from 37.5700 RMSE/N with the BC to 28.2601 RMSE/N with the MDOBC, which indicates that both two wire rope tensions' vibrations are reduced and variations are more consistent. From the above, one can conclude that the performance of the five controllers is as follows: the MDOBC > the CDO based BC > the TDO based BC > the BC > the PI controller.

5. Conclusions

This study is primarily concerned with wire rope tension control methodology for hoisting systems. Since Coulomb frictions between two wire ropes and two corresponding moving head sheaves, as well as complicated coupled disturbances appear in the hoisting system, a novel nonlinear model considering these disturbances is constructed. A TDO and a CDO are designed to online estimate and compensate for them. As a result, a MDOBC is designed to coordinate two wire rope tensions. Comparative experimental results demonstrate that the proposed control methodology exhibits a better performance than the TDO based BC, the CDO based BC, a BC, and a conventional PI controller.

Author Contributions: Conceptualization, W.Z. and J.Z.; methodology, W.Z. and X.C.; formal analysis, X.C. and J.Z.; writing—original draft preparation, W.Z.; writing—review and editing, X.C. and J.Z.; funding acquisition, W.Z. All authors have read and agreed to the published version of the manuscript.

Funding: This work was supported in part by Shandong Provincial Natural Science Foundation (Grant: ZR2021QE107, ZR2020QA044), in part by the National Natural Science Foundation of China (Grant: 52174144, 51774161, 51804151), in part by the Taishan scholar funding scheme (Grant: tsqn201909113).

Conflicts of Interest: The authors declare that we have no financial and personal relationships with other people or organizations that can inappropriately influence our work; there is no professional or other personal interest of any nature or kind in any product, service and/or company that could be construed as influencing the position presented in, or the review of, the manuscript.

Nomenclature

$\gamma_i, i = 1, 2.$	the angle between the catenary wire rope and the upper plane
$F_{xi}, i = 1, 2.$	the force of the No. i hydraulic cylinder
$F_{zi}, i = 1, 2.$	the No. i wire rope tension
k_f	the stiff of the force detector
$x_{pi}, i = 1, 2.$	the displacement of the No. i hydraulic cylinder
$x_{pfi}, i = 1, 2.$	the displacement of the No. i movable head sheave
$\Delta_i, i = 1, 2.$	the disturbance in the force dynamics
A_p	the effective area of chamber
$P_{Li}, i = 1, 2.$	the load pressure

$m_i, i = 1, 2.$	the load mass
$B_{pi}, i = 1, 2.$	the damping coefficient
$d_{hi}, i = 1, 2.$	the total disturbance in the speed dynamics
d_{12}, d_{21}	the coupled disturbances
$Q_{Li}, i = 1, 2.$	the load flow from the valve to the actuator chambers
$C_{tli}, i = 1, 2.$	the total leakage coefficient
$V_{ti}, i = 1, 2.$	the total volume
$x_{vi}, i = 1, 2.$	the spool displacement of servo valves
C_d	the discharge coefficient of servo valves
w	the throttle area gradient of servo valves
ρ_o	the density of the supply oil
p_s	the supply pressure
u_{Li}	the control voltage of servo valves
Q_r	the rated flow under the rated load pressure Δp_r
u_{\max}	the maximum control voltage
$x_i = [x_{i1}, x_{i2}, x_{i3}]^T, i = 1, 2.$	the state variables
$\theta_i, i = 1, 2.$	$k_f / (1 + \sin \gamma_i)$
$\theta_{i1}, i = 1, 2.$	A_p / m_i
$\theta_{i2}, i = 1, 2.$	B_{pi} / m_i
$\theta_{i3}, i = 1, 2.$	$1 / m_i$
$\theta_{i4}, i = 1, 2.$	$4A_p \beta_e / V_{ti}$
$\theta_{i5}, i = 1, 2.$	$4C_{tli} \beta_e / V_{ti}$
$\theta_{i6}, i = 1, 2.$	$4\beta_e / V_{ti}$
$\vartheta_i, i = 1, 2.$	the maximum bounded value of $ \Delta_i $
$\zeta_i, i = 1, 2.$	the maximum bounded value of $ d_{hi} $
$v_i, i = 1, 2.$	the maximum bounded value of $ \dot{\Delta}_i $
$v_i, i = 1, 2.$	the maximum bounded value of $ \dot{d}_{hi} $
$\hat{\Delta}_i, i = 1, 2.$	the estimation of Δ_i
$\tilde{\Delta}_i, i = 1, 2.$	the estimation error
$\xi_i, i = 1, 2.$	an auxiliary variable
$p(x_{i1}, x_{i2}), i = 1, 2.$	a function that needs to be designed
$\lambda_i, i = 1, 2.$	the control gain of the TDO
$\tilde{\Delta}_i, i = 1, 2.$	the estimation error dynamics
$\dot{\hat{\Delta}}_i, i = 1, 2.$	the estimation value dynamics
$\hat{d}_{hi}, i = 1, 2.$	the estimation value of d_{hi}
$\hat{x}_{i2}, i = 1, 2.$	the estimation value of x_{i2}
$A = [k_{d11}, k_{d12}; k_{d21}, k_{d22}]$	the control gain matrix of the CDO
$\hat{d}_{hi}, i = 1, 2.$	the dynamics of the estimation value of the CDO
$\dot{\tilde{d}}_{hi}, i = 1, 2.$	the estimation error dynamics of the CDO
$e = [e_{i1}, e_{i2}, e_{i3}], i = 1, 2.$	the system tracking error matrix
$e_{i1}, i = 1, 2.$	two wire rope tension tracking errors
$e_{i2}, i = 1, 2.$	two displacement velocity tracking errors
$e_{i3}, i = 1, 2.$	two load pressure tracking errors
$\alpha_{i1}, \alpha_{i2}, i = 1, 2.$	the virtual control laws
H_r	a bounded hypersphere ball
δ_i	$k_{dii} - 1/4k_{i2}$
$\chi_{ij}, i = 1, 2; j = 1, 2, 3.$	the Lyapunov functions
$\dot{\chi}_{ij}, i = 1, 2; j = 1, 2, 3.$	the time derivative of the Lyapunov functions
$K_{pi}, i = 1, 2.$	the control gains of the PI controller
$K_{li}, i = 1, 2.$	the control gains of the PI controller

Appendix A

The TDO Stability Proof. Define a Lyapunov function as

$$\chi_T = \tilde{\Delta}_i^2/2. \tag{A1}$$

and with results of Equation (10), its time derivative yields

$$\dot{\chi}_T = \tilde{\Delta}_i \dot{\tilde{\Delta}}_i = -\tilde{\Delta}_i \tilde{\Delta}_i / \lambda_i = -\tilde{\Delta}_i^2 / \lambda_i. \tag{A2}$$

Therefore, if the control gain λ_i are properly selected such that $\lambda_i > 0$, $\dot{\chi}_T \leq 0$ and then the estimation error will converge to a bounded small value. The TDO is stable. \square

The CDO Stability Proof. The estimation error dynamics of the CDO yields

$$\begin{bmatrix} \dot{\tilde{d}}_{h1} & \dot{\tilde{d}}_{h2} \end{bmatrix}^T = \mathbf{A} \underbrace{\begin{bmatrix} \tilde{d}_{h1} & \tilde{d}_{h2} \end{bmatrix}^T}_{s1} - \underbrace{\begin{bmatrix} \dot{d}_{h1} & \dot{d}_{h2} \end{bmatrix}^T}_{s2}. \tag{A3}$$

In Equation (A3), there are only two variables in the estimation error dynamics, i.e., \dot{d}_{hi} and \tilde{d}_{hi} . Therefore, if Equation (A3) is considered as a system, \dot{d}_{hi} is the input of the system and \tilde{d}_{hi} is the output. The time integral of Equation (A3) yields

$$\tilde{d}_{hi}(t) = \underbrace{e^{\mathbf{A}t} \tilde{d}_{hi}(0)}_{part\ 1} - \underbrace{\int_0^t e^{\mathbf{A}(t-\tau)} \dot{d}_{hi}(\tau) d\tau}_{part\ 2}. \tag{A4}$$

where, the *part 1* and the *part 2* are the integral of the $s1$ and the $s2$, respectively. Since \mathbf{A} is a Hurwitz matrix, the *part 1* is an exponential convergence term. If the initial estimation error is defined as $|\tilde{d}(0)| = \sqrt{\tilde{d}_{h1}^2(0) + \tilde{d}_{h2}^2(0)}$, thus,

$$\left| e^{\mathbf{A}t} \tilde{d}_{hi}(0) \right| \leq 2\sigma_{\min}(\mathbf{A}^{-1}) |\tilde{d}(0)|. \tag{A5}$$

where, $\sigma_{\min}(\mathbf{A}^{-1})$ is the min value among $\sigma_i(\mathbf{A}^{-1})$. Since

$$0 < \sigma_{\min}(\mathbf{A}^{-1}) \leq \sigma_i(\mathbf{A}^{-1}), \tag{A6}$$

therefore,

$$\left| e^{\mathbf{A}t} \tilde{d}_{hi}(0) \right| \leq 2\sigma_i(\mathbf{A}^{-1}) |\tilde{d}(0)|. \tag{A7}$$

Let $\lambda_{hi}(t) = -\int_0^t e^{\mathbf{A}(t-\tau)} \dot{d}_{hi}(\tau) d\tau$ and define $\dot{d}_{\max} = \sqrt{\dot{d}_{h1\max}^2 + \dot{d}_{h2\max}^2}$; one can obtain

$$\begin{aligned} |\lambda_{hi}(t)| &\leq \left\{ \left| \left[\mathbf{A}^{-1} \dot{d}(t) \right]_i \right| + \left| \left[\mathbf{A}^{-1} e^{\mathbf{A}t} \dot{d}(t) \right]_i \right| \right\} \\ &\leq \dot{d}_{\max} [\sigma_i(\mathbf{A}^{-1}) + \sigma_i(\mathbf{A}^{-1}) |e^{\mathbf{A}t}|_i] \leq \dot{d}_{\max} [\sigma_i(\mathbf{A}^{-1}) + 2\sigma_i^2(\mathbf{A}^{-1})] \end{aligned} \tag{A8}$$

Therefore, with the results of Equations (A7) and (A8),

$$\begin{aligned} \left| \tilde{d}_{hi}(t) \right| &= \left| e^{\mathbf{A}t} \tilde{d}_{hi}(0) \right| + \left| \int_0^t e^{\mathbf{A}(t-\tau)} \dot{d}_{hi}(\tau) d\tau \right| \\ &\leq 2\sigma_i(\mathbf{A}^{-1}) |\tilde{d}(0)| + \dot{d}_{\max} [\sigma_i(\mathbf{A}^{-1}) + 2\sigma_i^2(\mathbf{A}^{-1})] \\ &= \sigma_i(\mathbf{A}^{-1}) \left[2|\tilde{d}(0)| + \dot{d}_{\max} + 2\dot{d}_{\max} \sigma_i(\mathbf{A}^{-1}) \right] \end{aligned} \tag{A9}$$

As long as the diagonal control gains k_{dii} , $i = 1, 2$. In A are adjusted to be large enough and A is dominated by its diagonal elements, singular values $\sigma_i(A^{-1})$ will become small gradually with enlarging control gains k_{dii} , $i = 1, 2$. Therefore, the CDO is bounded stable. \square

References

1. Tanaka, K.; Nishimura, M.; Wang, H.O. Multi-objective fuzzy control of high rise/high speed elevators using LMIs. In Proceedings of the American Control Conference, Philadelphia, PA, USA, 26 June 1998; pp. 3450–3454.
2. Zhu, Z.; Li, X.; Shen, G.; Zhu, W. Wire rope tension control of hoisting systems using a robust nonlinear adaptive backstepping control scheme. *ISA Trans.* **2018**, *72*, 256–272. [[CrossRef](#)] [[PubMed](#)]
3. Zang, W.; Shen, G.; Rui, G.; Li, X.; Li, G.; Tang, Y. A flatness-based nonlinear control scheme for wire tension control of hoisting systems. *IEEE Access* **2019**, *7*, 146428–146442. [[CrossRef](#)]
4. Ma, H.; Tang, G.Y.; Hu, W. Feedforward and feedback optimal control with memory for offshore platforms under irregular wave forces. *J. Sound Vib.* **2009**, *328*, 369–381. [[CrossRef](#)]
5. Lee, S.G. Modeling and advanced sliding mode controls of crawler cranes considering wire rope elasticity and complicated operations. *Mech. Syst. Signal Process.* **2018**, *103*, 250–263.
6. Zhang, D.; Wu, Q.; Yao, X.; Jiao, L. Active disturbance rejection control for looper tension of stainless steel strip processing line. *J. Control Eng. Appl. Inform.* **2018**, *20*, 60–68.
7. Lu, J.S.; Cheng, M.Y.; Su, K.H.; Tsai, M.C. Wire tension control of an automatic motor winding machine—an iterative learning sliding mode control approach. *Robot. Comput. Integr. Manuf.* **2018**, *50*, 50–62. [[CrossRef](#)]
8. Li, X.; Zhu, Z.; Shen, G. A switching-type controller for wire rope tension coordination of electro-hydraulic-controlled double-rope winding hoisting systems. *Proc. Inst. Mech. Eng. Part I J. Syst. Control Eng.* **2016**, *230*, 1126–1144. [[CrossRef](#)]
9. Chen, X.; Zhu, Z.; Shen, G.; Li, W. Tension coordination control of double-rope winding hoisting system using hybrid learning control scheme. *Proc. Inst. Mech. Eng. Part I J. Syst. Control Eng.* **2019**, *233*, 1265–1281. [[CrossRef](#)]
10. Chen, X.; Zhu, Z.; Li, W.; Shen, G. Fault-tolerant control of double-rope winding hoists combining neural-based adaptive technique and iterative learning method. *IEEE Access* **2019**, *7*, 50476–50491. [[CrossRef](#)]
11. Zhao, J.; Na, J.; Gao, G. Adaptive dynamic programming based robust control of nonlinear systems with unmatched uncertainties. *Neurocomputing* **2020**, *35*, 56–65. [[CrossRef](#)]
12. Sariyildiz, E.; Ohnishi, K. An adaptive reaction force observer design. *IEEE/ASME Trans. Mechatron.* **2014**, *20*, 750–760. [[CrossRef](#)]
13. He, H.; Na, J.; Huang, Y.; Liu, T. Integrated Modeling and Adaptive Parameter Estimation for Hammerstein systems with Asymmetric Dead-Zone. *IEEE Trans. Ind. Electron.* **2022**. [[CrossRef](#)]
14. Na, J.; Zhao, J.; Gao, G.; Li, Z. Output-feedback robust control of uncertain systems via online data-driven learning. *IEEE Trans. Neural Netw. Learn. Syst.* **2021**, *32*, 2650–2662. [[CrossRef](#)] [[PubMed](#)]
15. Sariyildiz, E.; Ohnishi, K. On the explicit robust force control via disturbance observer. *IEEE Trans. Ind. Electron.* **2014**, *62*, 1581–1589. [[CrossRef](#)]
16. Na, J.; Li, Y.; Huang, Y.; Gao, G.; Chen, Q. Output feedback control of uncertain hydraulic servo systems. *IEEE Trans. Ind. Electron.* **2019**, *67*, 490–500. [[CrossRef](#)]
17. Na, J.; He, H.; Huang, Y.; Dong, R. Adaptive estimation of asymmetric dead-zone parameters for sandwich systems. *IEEE Trans. Control Syst. Technol.* **2021**, *30*, 1336–1344. [[CrossRef](#)]
18. Xiao, L.; Lu, B.; Yu, B.; Ye, Z. Cascaded sliding mode force control for a single-rod electrohydraulic actuator. *Neurocomputing* **2015**, *156*, 117–120. [[CrossRef](#)]
19. Roy, S.; Baldi, S.; Fridman, L.M. On adaptive sliding mode control without a priori bounded uncertainty. *Automatica* **2020**, *111*, 108650. [[CrossRef](#)]
20. Wang, J.; Zhu, P.; He, B.; Deng, G.; Zhang, C.; Huang, X. An adaptive neural sliding mode control with ESO for uncertain nonlinear systems. *Int. J. Control Autom. Syst.* **2020**, *19*, 687–697. [[CrossRef](#)]
21. Won, D.; Kim, W.; Shin, D.; Chung, C.C. High-gain disturbance observer-based backstepping control with output tracking error constraint for electro-hydraulic systems. *IEEE Trans. Control Syst. Technol.* **2014**, *23*, 787–795. [[CrossRef](#)]
22. Tee, K.P.; Ge, S.S.; Tay, E.H. Barrier Lyapunov functions for the control of output-constrained nonlinear systems. *Automatica* **2009**, *45*, 918–927. [[CrossRef](#)]
23. He, W.; Sun, C.; Ge, S.S. Top tension control of a flexible marine riser by using integral-barrier Lyapunov function. *IEEE/ASME Trans. Mechatron.* **2014**, *20*, 497–505. [[CrossRef](#)]
24. Zang, W.; Zhang, Q.; Shen, G.; Fu, Y. Extended sliding mode observer based robust adaptive backstepping controller for electro-hydraulic servo system: Theory and experiment. *Mechatronics* **2022**, *85*, 102841. [[CrossRef](#)]
25. Sariyildiz, E.; Oboe, R.; Ohnishi, K. Disturbance observer-based robust control and its applications: 35th anniversary overview. *IEEE Trans. Ind. Electron.* **2019**, *67*, 2042–2053. [[CrossRef](#)]
26. Wei, X.J.; Wu, Z.J.; Karimi, H.R. Disturbance observer-based disturbance attenuation control for a class of stochastic systems. *Automatica* **2016**, *63*, 21–25. [[CrossRef](#)]
27. Kai, G.; Wei, J.; Fang, J.; Feng, R.; Wang, X. Position tracking control of electro-hydraulic single-rod actuator based on an extended disturbance observer. *Mechatronics* **2015**, *27*, 47–56.

28. Besnard, L.; Shtessel, Y.B.; Landrum, B. Quadrotor vehicle control via sliding mode controller driven by sliding mode disturbance observer. *J. Frankl. Inst.* **2012**, *349*, 658–684. [[CrossRef](#)]
29. Lu, Y.S. Sliding-mode disturbance observer with switching-gain adaptation and its application to optical disk drives. *IEEE Trans. Ind. Electron.* **2009**, *56*, 3743–3750.
30. Zhang, J.; Liu, X.; Xia, Y.; Zuo, Z.; Wang, Y. Disturbance observer-based integral sliding-mode control for systems with mismatched disturbances. *IEEE Trans. Ind. Electron.* **2016**, *63*, 7040–7048. [[CrossRef](#)]
31. Chen, M.; Shi, P.; Lim, C.C. Robust constrained control for MIMO nonlinear systems based on disturbance observer. *IEEE Trans. Autom. Control* **2015**, *60*, 3281–3286. [[CrossRef](#)]
32. Zheng, M.; Lyu, X.; Liang, X.; Zhang, F. A generalized design method for learning-based disturbance observer. *IEEE/ASME Trans. Mechatron.* **2021**, *26*, 45–54. [[CrossRef](#)]
33. Rashad, R.; El-Badawy, A.; Aboudonia, A. Sliding mode disturbance observer-based control of a twin rotor MIMO system. *ISA Trans.* **2017**, *69*, 166–174. [[CrossRef](#)] [[PubMed](#)]
34. Ginoya, D.; Shendge, P.D.; Phadke, S.B. Disturbance observer based sliding mode control of nonlinear mismatched uncertain systems. *Commun. Nonlinear Sci. Numer. Simul.* **2015**, *26*, 98–107. [[CrossRef](#)]
35. Deng, Y.; Wang, J.; Li, H.; Liu, J.; Tian, D. Adaptive sliding mode current control with sliding mode disturbance observer for PMSM drives. *ISA Trans.* **2019**, *88*, 113–126. [[CrossRef](#)] [[PubMed](#)]
36. Zhang, C.; Chen, Z.; Wei, C. Sliding mode disturbance observer-based backstepping control for a transport aircraft. *Sci. China Inf. Sci.* **2013**, *57*, 1–16. [[CrossRef](#)]
37. Guo, Q.; Yin, J.M.; Yu, T.; Jiang, D. Coupled-disturbance-observer-based position tracking control for a cascade electro-hydraulic system. *ISA Trans.* **2017**, *68*, 367–380. [[CrossRef](#)] [[PubMed](#)]
38. Thompson, J.O. Hooke's law. *Science* **1926**, *64*, 298–299. [[CrossRef](#)]
39. Chen, W.H.; Yang, J.; Guo, L.; Li, S. Disturbance-observer-based control and related methods—An overview. *IEEE Trans. Ind. Electron.* **2016**, *63*, 1083–1095. [[CrossRef](#)]
40. Chen, W.H.; Ballance, D.J.; Gawthrop, P.J.; O'Reilly, J. A nonlinear disturbance observer for robotic manipulators. *IEEE Trans. Ind. Electron.* **2000**, *47*, 932–938. [[CrossRef](#)]